An Integrated Particle Sampler and Lung Radiation Dosimeter

J. K. C. Leung, M. Y. W. Tso, S. H. Li, H. C. Lam, A. S. Poon, D. T. Xiao, and Q. F. Zhou

***Abstract*—A lung dosimeter that can record the nonradiological hazard of aerosol particles to the lung as well as the radiological hazard of air borne radionuclides that are attached to aerosol particles has been developed. The dosimeter is capable of recording aerosol particles of diameters from 10^{-2} μm to 10^{2} μm by electrostatic collection in a specially designed dosimeter body. The aerosol size distribution is recorded on a mylar strip and the activity size distribution of α, β, and γ radiation emitting aerosols are recorded on another strip coated with α-Al_2O_3:C. Both strips can be read by a specially built reader, the output of which can be used to calculate the nonradiological hazard and radiological hazard, respectively, and to give an overall picture of the exposure.**

***Index Terms*—Dosimetry, respiratory system, particle measurement, thermoluminescence.**

I. Introduction

THE RESPIRATORY tract is an important route for radionuclides and other hazardous airborne materials to enter the body. The inhalation of airborne particulates and the subsequent hazard, both radiological and nonradiological, is determined by numerous physical, chemical, and biological factors. Out of these factors, the size of the particulates is probably the most critical in determining how and where the particulates will deposit along the respiratory tract.

In the early 1990s, international committees from ISO (1983) [1], CEN (1993) [2], and the ACGIH (1996) [3] developed a new size convention to define the sampling criteria for all health-based particle sampling. Particles are now divided into three health related size fractions: inhalable, thoracic, and respirable and exposure standards will be based on concentration limits in one or more of these size fractions. The efficiency for collecting the three size fractions should now follow the size conventions given in Fig. 1.

There are many ways to separate particles of different sizes. Each method has its own sampling efficiency curve that may differ from the conventions. Some sampling methods require separate samples for separate measurement of the three size fractions, while others may be able to separate a single sample into the three size fractions for simultaneous measurements [4]. Some of these methods are described as follows.

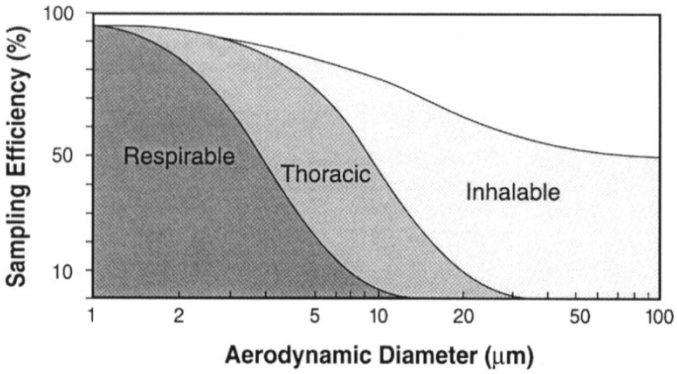

Fig. 1. Size convention curves.

1) Filter sampler—A filter is probably the simplest air borne particle sampler. Different designs aim at collecting different size fractions. But so far, filter samplers are only useful for measuring total aerosol or aerosols in the inhalable fraction.
2) Porous foam—The porous foam acts similar to a filter, but is capable of separating the respirable size fraction. A drawback is that the uniformity of the foam media is not satisfactory and more work is required to develop a foam of adequate uniformity.
3) Impactors—Particles in the air stream are passed through a nozzle and impacted onto a flat impaction plate. The air stream is bent 90° and only particles smaller than a certain size can follow the air stream while the larger particles will leave the stream, hit the impaction plate and stick. The remaining particles in the air stream can be further separated by flowing through a stack of impactors, each having a different cut-point. There are several problems associated with conventional impactors. Firstly the sampling efficiencies do not match the conventions. This becomes worse as particles build up on the impaction surface and affect the streamline and size cut-off of the impactor. Secondly, the particles collected on the impaction surface may bounce off and be re-entrained into the flow.
4) Virtual impactor [5]—A virtual impactor is a device that separates particles by size into two air streams. It is similar to a conventional impactor, but the impaction surface is replaced with a virtual space of stagnant or slow moving air. Large particles are captured in a collection

Manuscript received August 1, 2002. This work was supported in part by the Hong Kong Research Grant Council.

J. K. C. Leung is with the Department of Physics, The University of Hong Kong, Hong Kong, China (e-mail: jkcleung@hku.hk).

M. Y. W. Tso is with the Safety Office, The University of Hong Kong, Hong Kong, China.

S. H. Li is with the Department of Earth Sciences, The University of Hong Kong, Hong Kong, China (e-mail: shli@hkusua.hku.hk).

H. C. Lam is with the Department of Physics, The University of Hong Kong, Hong Kong, China (e-mail: lamhc@hkusua.hku.hk).

A. S. Poon is with the Department of Physics, The University of Hong Kong, Hong Kong, China.

D. T. Xiao is with the School of Nuclear Science and Technology, Nanhua University, Hunan, China (e-mail: dt_xiao@21cn.com).

Q. F. Zhou is with the Laboratory of Industrial Hygiene, Ministry of Health, Beijing, China.

Digital Object Identifier 10.1109/TNS.2003.812442

probe rather than impacted onto a surface. By cascading the virtual impactors, the particles can be separated into the different size fractions. A major difference between a virtual impactor and an impactor is that the smaller particles are removed from the air stream first, leaving the largest particles to be collected last. This is contrary to an impactor where the largest particles are separated from the air stream first.

5) Electrostatic classifier [6]—Aerosols are first charged by an ionizer or ionizing radiations. They are then deflected by a static electric field toward a collector. By changing the magnitude of the electric field, different size of particulates will be collected according to their difference in mobility. One drawback of this technique is that a complicated controlling system is required.

At more or less the same time, the International Commission on Radiological Protection has also proposed a new human respiratory tract model for calculating the deposition of radioactive aerosol along the human respiratory tract and for assessing the radiation dose arising from the inhalation [7]. The radioactive aerosols are assumed to have a log-normal size distribution which is characterized by the activity median aerodynamic diameter (AMAD) and the geometric standard deviation (GSD). The size distribution of air borne particulates and activity size distribution of radioactive airborne particulates are in general unrelated except for radon progenies and volatile radionuclides which attach themselves to airborne particulates [8]. Hence the AMAD is a separate parameter from the size fractions and has to be determined separately if inhalation radiation dose is a concern. However, the AMAD is much more difficult to be determined than size distribution. For radon progenies that attach themselves to airborne particulates, it is generally assumed that the activity size distribution is related to the size distribution of the airborne particulates by the attachment coefficients [8] and thus can be obtained by a measurement of the latter. For radiation workers who may be exposed to radioactive aerosol whose size distribution is determined by the isotopes themselves, the radioactive aerosol has to be sampled in a number of size ranges and the individual activities measured separately to determine the overall activity size distribution. Normal discrete size sampler or electrostatic classifier can be used [9]. One major difficulty in sampling radioactive aerosol is that the radioactive half-life must be considered.

Radiation workers are also subjected to external irradiation from β or γ radiations. For the measurement of the integrated external radiation dose, the TLD is the most commonly used passive dosimeter. But recently, optically stimulated luminescence (OSL) dosimeters are available in the market and are slowly gaining popularity.

So far, the radiological and nonradiological exposures are measured by separate equipment and it is difficult to correlate the separate results to give an overall picture of the exposure. In this paper, an integrated particle sampler and radiation dosimeter that will record the particle size fractions, the lung radiation dose due to inhalation and the external radiation dose simultaneously will be presented. The readout system and data manipulation will also be discussed. Since the dosimeter can record radiological and nonradiological exposures, it could be installed in radioisotope laboratories where risk of inhalation and external dose are high or in mines where nonradiological exposure is equally important.

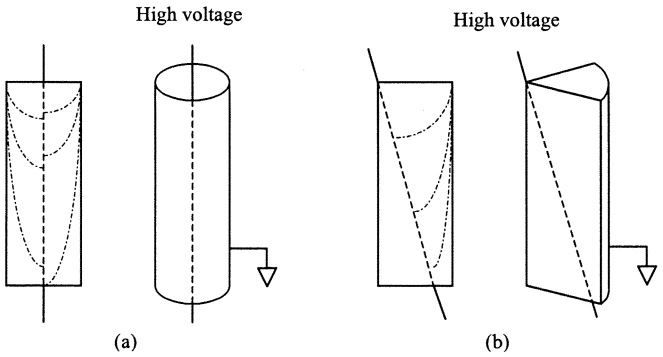

Fig. 2. (a) Normal configuration of an electrostatic classifier. (b) Modified configuration with a slanting central electrode.

II. Method

A. Dosimeter Body

The separation of different sizes of aerosol particles by electrostatic means has been widely applied. One of these techniques is to inject the charged aerosol along the perimeter of a conducting cylinder and applying a high voltage to a conducting central rod which attracts the aerosol particles toward it. The transverse movement of the particles is dependent on the applied voltage and the charge and mass of the particle (the mobility). The core of the air stream is filled with a controlled flow of aerosol-free air that maintains laminar airflow inside the cylinder. A schematic diagram of this electrostatic classifier is shown in Fig. 2. However, there are a number of drawbacks in this design if we want to sample the aerosols by collecting them at the central rod. Firstly, the size of collected aerosol along the central rod is far from linear and secondly an extremely high voltage is required if particles above μm diameter are to be collected. In this paper, a modified design of the classifier is used which is capable of collecting and measuring the size distribution and activity size distribution of airborne aerosols for particle diameters of 10^{-2} μm up to 10^{2} μm. The schematic diagram is also shown in Fig. 2. The cylindrical core is replaced by a segment of a cylinder while the central electrode becomes a slanting detector strip (to be discussed later). This set-up allows the low mobility (large) aerosol particles to fall onto the detector in addition to being attracted toward it by the electric field, thus extending the detectable size range. The aerosols will enter the dosimeter through a small dome-shaped chamber at the top of the dosimeter body, where the larger particles will be filtered, simulating the human nose and mouth. The "inhalable" fraction of particles will enter the dosimeter body along the arc of the body which is coated with a layer of conducting material to form the ground electrode. Filtered sheath air flows in the rest of the dosimeter body to maintain laminar flow. As the aerosol particles flow downwards, they will get closer to the electrode and will experience a stronger attractive force. In order to eliminate the difference in distance from the electrode to aerosol particles that entered at different positions along the arc, a sophis-

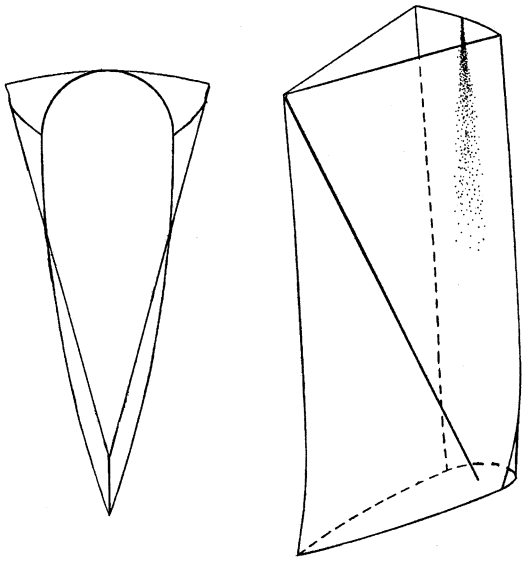

(a) (b)

Fig. 3. (a) Transverse view of the dosimeter body showing the changing cross sections. (b) Outline of the dosimeter body and the illustrated flow of particles without the transverse electric field.

ticated computer designed dosimeter body was built as shown in Fig. 3. The principles of the design are: 1) to maintain the detector (central electrode) as the center of the arc (circumference electrode) at all transverse sections; 2) to maintain the arc length unchanged at all transverse sections, and 3) to maintain the perimeter and cross-sectional area of all transverse sections the same.

The idea is to maintain a constant velocity laminar flow inside the dosimeter body while pushing the larger aerosol particles toward the detector as they flow downward by curving the arc. In the prototype dosimeter, the starting subtended angle of the arc is 30° and ends up with a maximum of 180°. The design has been proved to be successful by water flow experiments where a transparent dosimeter body was built with Perspex and fine charcoal powders were injected into the water flow to simulate the aerosol particles. The stream of powders was drawn in the dosimeter body in Fig. 3 for illustration purposes. Inevitably the flow near the detector and the bottom of the dosimeter body will be turbulent, but this does not seem to be a disadvantage because the turbulence allows even very large particles to be captured by the detector.

In order to make the inlet aerosol charged, an ionizer was installed at the entrance of the dosimeter body. A high voltage applied to the fine carbon fibers of the ionizer will breakdown air molecules at the end of the fibers, thus providing a source of electrons for the incoming aerosol particles.

The electrical mobility, Z ($m^2s^{-1}V^{-1}$) of a particle is defined as the electrical velocity component v (ms^{-1}) of the particle per unit electric field strength, E (Vm^{-1}), i.e., $Z = v/E$. Under an equilibrium condition between the electrical force and the fluid drag force, it can be shown that electrical mobility can be given by

$$Z = K\frac{n}{D}$$

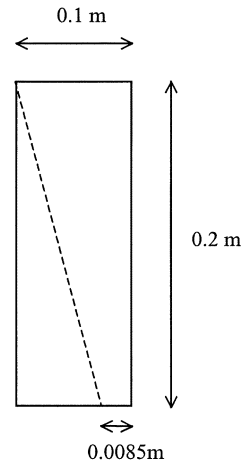

Fig. 4. Dimensions of the prototype dosimeter.

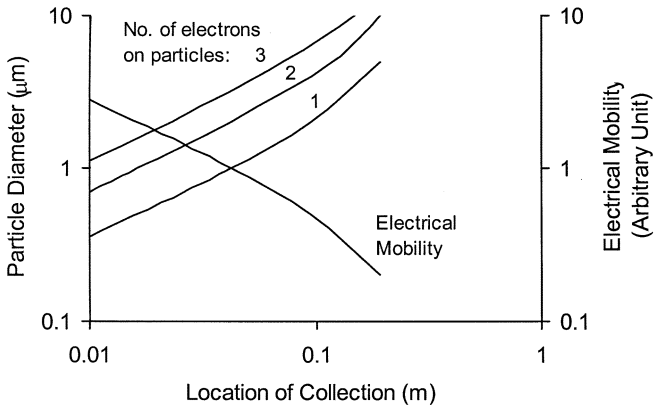

Fig. 5. Change in mobility and diameter of the collected aerosol particles along the length of the detector.

where n is the number of electronic charges carried by the particle of diameter D and K is a constant which is dependent on the gas viscosity and the Cunningham slip correction.

When the aerosol particles enter the dosimeter body, they will first be ionized by the ionizer at the inlet and then attracted toward the detector by the electric field. For design purposes, it was assumed that only the transverse velocity component of the particles would be affected by the electric field while the longitudinal component remains constant. Numerical iteration method was then used to find out at which point on the detector would a particular particle deposit, hence to find the distribution of particle mobility along the detector. For the prototype dimension as shown in Fig. 4 and at a high voltage of 1000 V and an air flow speed of 0.08 ms^{-1}, the distribution of mobility along the detector was calculated as shown in Fig. 5.

Since multiple charges can exist on an aerosol particle and this probability is particle size dependent, it is not possible to do a one-to-one mapping to determine the size of a deposited particle by referring to its mobility. The size distribution of multiply-charged particles along the detector is also shown in Fig. 5. Table I gives the distribution of charges on aerosol particles according to Boltzmann's equilibrium [10]. It can be seen that most small particles will be neutral while large particles can

TABLE I
DISTRIBUTION OF CHARGES ON AEROSOL PARTICLES ACCORDING TO BOLTZMANN'S EQUILIBRIUM

Particle	Percent of particles carrying n charges								
Diameter (μm)	n = -4	-3	-2	-1	0	1	2	3	4
0.01				0.34	99.32	0.34			
0.10		0.26	4.39	24.09	42.52	24.09	4.39	0.26	
1.00	5.42	8.06	10.71	12.70	13.45	12.70	10.71	8.06	5.42

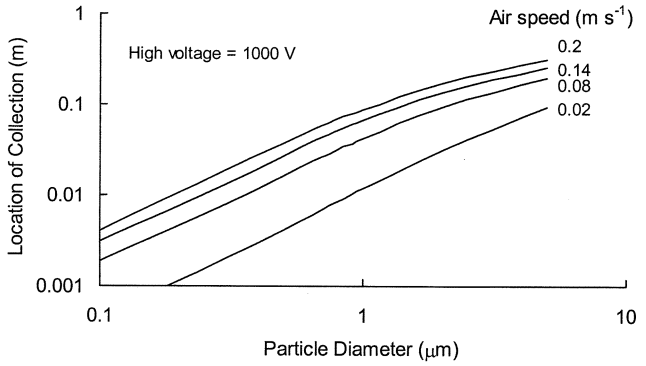

Fig. 6. Location of collection of different sized particles at different air speeds inside the dosimeter body.

carry up to a few charges of either polarity under a charge equilibrium state. The ionizer at the entrance of the dosimeter body is used to charge up all the aerosol particles instead of neutralizing their charges, so it is expected that most of the particles will at least carry one charge. The actual distribution of particle size along the detector will therefore need to be studied and detailed results will be published separately.

For singly charged aerosol particles, their deposition locations as a function of the speed of airflow inside the dosimeter body are calculated and shown in Fig. 6. In order to collect a wide range of aerosol size with reasonable collection efficiency, the applied high voltage and the speed of flow inside the dosimeter body must be compromised. For our prototype detector, a high voltage of 1000 V and a flow speed of 0.08 ms^{-1} were chosen as illustrated in Fig. 6.

B. Detector

The detector serves to measure the size distribution and activity size distribution of the aerosols. It consists of two strips: a strip of transparent mylar having a thickness of 0.0835 mg cm^{-2} and a strip of 0.4 mm thick aluminum coated on both sides with OSL powders (α-Al_2O_3:C) as shown in Fig. 7. A stainless steel wire of diameter 50 μm is sandwiched between the two strips and acts as the electrode. Amounts of 2 to 3 kV may be applied to this electrode to attract the charged aerosol particles to deposit on the mylar strip. Radiations emitted from the deposited aerosol particles can penetrate the mylar and be recorded by the OSL strip. The OSL on the front side of the OSL strip will record all α, β, and γ dose if present while the back side will record high energy β and γ because of the presence of the aluminum backing. After exposure, both strips can be taken out and inserted into a specially designed and built reader (to be discussed in a later section) to readout the signals. The aerosol size distribution is determined by measuring the transparency along the mylar strip, inferring the

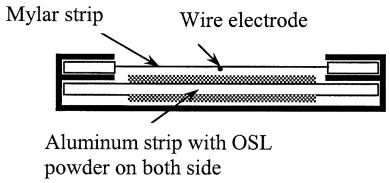

Fig. 7. Cross-sectional view of the detector holder.

amount of deposition for each size range. Similarly, the activity size distribution of the radioactive aerosol particles and the cumulative α, β and γ dose are determined by reading out the OSL signals recorded along both sides of the OSL strip.

C. OSL Strip

The use of α-Al_2O_3:C for TL and OSL dosimetry has been widely studied [11], [12] which shows that this material, whether in single crystal, powders, or thin layers on substrates is a very good TL phosphors. Though thermal quenching i.e., the reduction of the TL signal at elevated heating rates [13] and extremely high light sensitivity [14] of α-Al_2O_3:C has prevented its use for routine TL dosimetry, its high light sensitivity has led to its successful applications in OSL dosimetry. The α-Al_2O_3:C crystal is grown in an oxygen deficit condition, which results in high concentrations of oxygen vacancy centers—the F and F^+ centers. The substitution of the trivalent Al^{3+} ions by divalent impurities such as C^{2+} or Mg^{2+} further enhances the existence of F^+ centers. The nominal number of F and F^+ centers are $1-5\times10^{17}cm^{-3}$ and $5-10\times10^{15}cm^{-3}$. After irradiation by ionizing radiation, electrons and holes in the dosimetric traps can be released by exposure to optical wavelengths. Released electrons will cause emission at 420 nm due to the reaction $e^- + F^+ \rightarrow F^* \rightarrow F + h\nu_{420}$ with a lifetime of $\sim$ 35 ms, where F^* represents an excited F center. Conversely, released holes will cause emission at 326 nm due to the conversion of F to F^+ according to the reaction $h^+ + F \rightarrow F^{+*} \rightarrow F^+ + h\nu_{326}$ and having a lifetime of less than 7 ns [15]. Electrons are released over a wide range of stimulation wavelengths, ranging from less than 200 nm UV to visible and infrared [16]. In this project, a laser producing 50 mW of 532 nm green light by Oriel Instrument was used as the stimulating light.

α-Al_2O_3:C single crystals in the form of TLD-500 were bought from Harshaw Chemical Co., Ltd. They were grounded and sieved into OSL powders of grain size from 75 to 90 μm. The crystal grains were first washed with HCl to remove possible contamination of metal powder during the grinding process and then rinsed with water and allowed to dry. About 0.3 g of OSL powder were bonded onto each surface of an aluminum strip (2.5 mm $\times$ 200 mm) by a special method.

Annealing of the OSL strip can be done by either heating the strip at high temperature or releasing all the trapped carriers by shining with intense visible or UV light. Heat annealing was used in this project and the heating temperature was 600 °C for 3 hours. Higher temperatures were not used because of the low melting point of Al at about 660 °C.

D. Sensitivity of the OSL Strip

It is noted in the previous section that the sensitivity of the OSL strip is strongly dependent on the F^+ center concentration, where the trapped electrons will recombine to produce the 420 nm emissions after being released by the optical stimulation. Though radiation can increase F^+ center concentration through the $h^+ + F \rightarrow F^+$ reaction, the number of radiation-induced F^+ centers is likely to be many orders of magnitude smaller than the number of pre-existing F^+ centers, which are produced and determined by the crystal growth process. Because of this, the OSL crystal has a high sensitivity and linear dose response.

Another factor that determines the sensitivity of the OSL strip is its transparency to the stimulation light and the 420 nm emission. When crushed into crystal grains and bonded to form the strip, the OSL powders become white in color. The transmission coefficients of the powder layers of different thickness were measured by a spectrophotometer and were found to be lower than that of the OSL crystals at both 532 nm and 420 nm photons, implying a lower sensitivity than the original crystal. This further implies that only the surface layer of the OSL film is stimulated to emit the 420 nm photons, and the deeper layers are either not stimulated or the emissions cannot escape.

The dose response of the OSL strip was studied by irradiating the strip to known β doses in an irradiator (Model 801 Multiple Sample Irradiator). The absorbed radiation dose was readout by stimulating the OSL strip with a 532 nm green laser pulse of width 0.25 s and then counting the 420 nm photons by a 30 mm diameter photomultiplier tube and fast photon counting system. The photomultiplier has a BG4 filter (280 –520 nm transmission window) at its entrance window to cut off the 532 nm photons coming from the laser. Detailed description of the reader is given in a later section. The dose response of the prototype reader was found to be about 1 counts/μGy for β^-, giving a minimum detectable β^- dose of about 30 μGy. This minimum dose could be lowered by using a stronger stimulating light or reading the strip for a more number of times. The dose response of α-Al_2O_3:C has been shown by many authors to be linear for doses ranging from as low as a few μGy up to 100 Gy [17]. The dose response of our OSL strip was also determined by irradiating the strip to either ^{90}Sr or ^{137}Cs for various exposure times. Results are shown in Fig. 8.

Two types of decay processes are observed in a pulsed OSL measurement. The first is the decay of luminescence with time for the recombination reaction $e^- + F^+ \rightarrow F^* \rightarrow F + h\nu_{420}$, which has a lifetime of $\sim$ 35 ms. On top of this main trap transitions, phosphorescence is observed when the charge carriers are retrapped by shallow traps. The phosphorescence is therefore temperature dependent and the lifetime is also temperature dependent and can vary from a few hundred to a few thousand milliseconds. The second decay process is the gradual decrease in the luminescence with the number of laser stimulation. Since

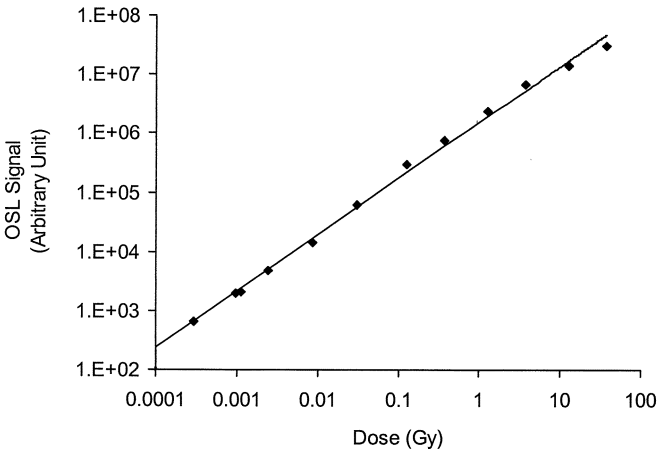

Fig. 8. Dose response of the OSL strip to radiations.

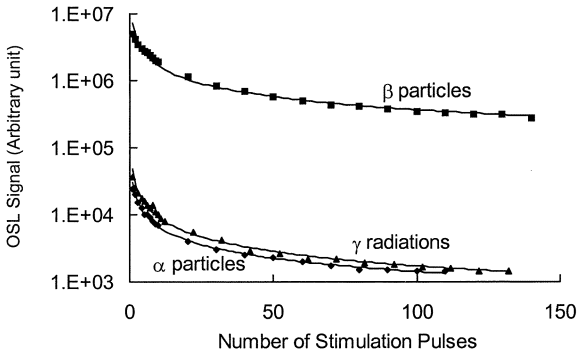

Fig. 9. Decrease of OSL signal with the number of stimulation light pulses.

a single pulse of stimulating light may not be sufficient to release all the trapped carriers, subsequent pulses can be used to readout the signals again but with less efficiency. The change in efficiency with number of readout pulses were studied for the OSL strip and the result is shown in Fig. 9. Because of the presence of the phosphorescence, sufficient time must be allowed for each subsequent stimulating pulse, or else the background will change. It is evidenced from Fig. 9 that the drop in OSL signal is independent of the type of irradiation. They can all be represented by power law equations with more or less the same exponent as shown by the lines in Fig. 9. Other authors have obtained different drop rate equations. For example Bulur and Goksu [12] found a linear relation and McKeever and Akselrod [11] found a double exponential relation. Hence, it is evidenced that the drop rate depends not only on the readout system such as the laser power and duration, but also on the configuration of the detector, whether in crystal form or powder form and on the method for fabricating the detector. It is also noted that both the sensitivity and drop rate of the OSL strip vary from strip to strip with a deviation of up to 8% for the sensitivity and up to 4% for drop rate. So it is important that the strips have to be carefully chosen if uniformity in dose response is required.

The detection efficiency of the OSL strip to different types of radiations were studied by irradiating the strip to known activities of α, β^-, β^+, and γ radiations. γ exposure was done in three different configurations of the OSL strip: one with the OSL grain facing the source and absorbing the radiation

TABLE II
RADIATION DOSE RESPONSE OF THE OSL STRIP TO DIFFERENT TYPES OF RADIATIONS

Radiation	Dose Response* (counts/μGy)	
	OSL strip	OSL crystal
α	$6.7 \times 10^{-3}\ \alpha^{-1}$	$0.014\ \alpha^{-1}$
β^-	2.0	--
β^+	8.5	--
γ (without Al plate)	1.8	--
γ (with incident Al plate)	2.1	--
γ (with 2 Al plates)	2.4	--

* Dose response for α-particles is expressed as counts per surface emissivity of the α source. All the values are not absolute and they can be improved by changing the laser pulse intensity, width and measurement timings, etc.
-- Not measured.

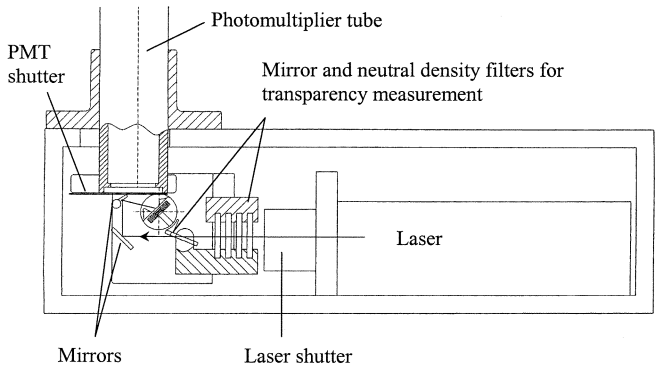

Fig. 10. Reader for reading both the transparency of the mylar strip and the radiation dose recorded in the OSL strip.

energy directly and the second with the aluminum backing of the strip facing the source, thus absorbing the γ radiation indirectly. The third configuration is to add one more piece of aluminum to sandwich the OSL layer between the two aluminum plates. The latter configuration is the design adopted in the lung dosimeter. The radioactive sources used in this experiment were: 1) 5.11 kBq ^{241}Am α source; 2) 7.4 GBq ^{90}Sr β^- source; 3) 126 MBq ^{137}Cs γ source; and 4) 20 keV β^+ emitted from a positron gun at a flux of 5000 β^+ $s^{-1}cm^{-2}$. The measured detection efficiencies are given in Table II. The doses in Table II, except for α-radiations, were all calibrated for tissue equivalent at a density of 1 g cm^{-3}. The α response is given as the OSL signal against the surface α emissivity of the source. It is evidenced that the OSL strip can have the best response when the OSL powders are sandwiched between two aluminum plates. The difference in dose response between OSL crystal and OSL strip is also illustrated in the table. Positron was found to give a larger dose response. This is largely attributed to its low energy of only 20 keV but it is also speculated that the β^+ might have changed the sensitivity of the OSL through converting F centers into F^+ centers. Moreover, the annihilation photons will also contribute to the dose. Further study in this aspect will be done to confirm the finding.

E. Reader

A particular feature of OSL dosimetry is the capability of partial readout of the signal, and this allows the OSL strip to be read repeatedly if required. The fraction of OSL signal released in each laser stimulation depends on the wavelength, intensity, and duration of the laser pulse. In theory, if an optical filter can be found that could totally block off the laser light while allowing the 420 nm and 326 nm OSL signals to pass through, then this filter can be put in front of a photomultiplier tube (PMT) to achieve collection of signal even during the light stimulation pulses. But in practice, no filter can 100% block out the stimulating light while maintaining a high transparency for the OSL signals, hence the signal is always measured after the stimulation pulse has gone. And because of this, short (millisecond order) intense laser pulses are preferred so as to reduce the loss of the 420 nm signals emitted during the stimulation.

A two-shutter system is adopted in our reader as shown schematically in Fig. 10. The PMT shutter operates out of phase with the laser shutter and there is a short delay of a few milliseconds between the opening of the PMT shutter and the closure of the laser shutter to allow for phosphorescence from the surrounding structure. The laser was a 50 mW cw solid state green laser manufactured by Oriel Instruments and the PMT was a 30 mm diameter end window PMT with blue-green sensitive bialkali photocathode and the AD6 amplifier-discriminator from Electron Tubes Limited.

Since the OSL strip is light sensitive, a special cartridge was designed for transportation and loading/unloading to or from the dosimeter and the reader. Once the cartridge is docked in the reader, the OSL strip will be drawn into the reader and read according to user's instruction, such as the reading positions, number of stimulating pulses, etc. After reading through one surface of the OSL strip, it will be turned over and the other surface read accordingly. The strip will be loaded back into the carrying cartridge after the readout process is completed. Similarly, the mylar strip can be unloaded from its cartridge and the transmission coefficient along the strip can be read by the same laser and PMT system except this time the laser beam is directed to pass through the strip instead of shining on the surface of it as is the case for the OSL strip. This is achieved by the movement of a mirror with the associated neutral density filter, which is used to cut down the laser intensity.

F. Analysis Program

A special program (will be described elsewhere) has been written to calculate: 1) the three health related size fractions: inhalable, thoracic, and respirable, according to the amount of aerosol particles collected along the mylar strip and 2) the radiation equivalent dose received in the lung according to the OSL signals recorded along the OSL strip. The lung dose model follows the ICRP Human Respiratory Tract Model [7] except that the Monte Carlo approach instead of the filter method was used. This allows us to trace every radioactivity-loaded aerosol particles inside the lung instead of using the AMAD value which sometimes does not truly represent the distribution, particularly for aerosols involved in the release of radioactive fume during an accident. Furthermore, for radionuclides in a decay series, the recoil energy from an α-decay is sufficient to eject the decay

product into the air stream inside the respiratory tract, hence will be transferred to other part of the lung. This has been shown by our program to result in a significant difference in equivalent dose to the lung; hence the Monte Carlo approach is a better representation of the true picture.

III. Conclusion

A dosimeter that can record simultaneously both radiological exposure and nonradiological exposure to the lung has been developed. The electrostatic classifier configuration is used for the collection of the charged aerosol particles onto a mylar strip. Radionuclides that are attached to the aerosol particles emit radiations and some of these radiations are recorded by a second strip coated with OSL (α-Al_2O_3:C) powders that is located right below the mylar strip. Coupled with the computer-aided design of the dosimeter body, the measurable size range of the aerosol particles is from 10^{-2} μm up to 10^2 μm. The distribution of aerosol particles along the mylar strip enables a precise computation of the three size fractions as shown in Fig. 1 to be obtained. Similarly, the distribution of absorbed dose along the OSL strip enables a precise computation of the deposition of the radionuclides in the lung, including the effect of radionuclide recoil, hence the equivalent dose to the lung can be obtained.

A number of these prototype dosimeters will be built and deployed in laboratories of The University of Hong Kong to test for its reliability and performance. The results of which can then be incorporated in the specification settings and fine-tuning of the final product.

References

[1] "Air quality – Particle size fraction definitions for health related sampling," Int. Standard Organization, ISO/TR 7708, 1983.

[2] "Size fraction definitions for measurement of airborne particles," Comite Europeen de Normalization (CEN), Brussels, Belgium, EN481:1993E, 1993.

[3] "1996 threshold limit values for chemical substances and physical agents, biological exposure indices," in Amer. Conf. Governmental Industrial Hygienists, Cincinnati, OH, 1996.

[4] J. H. Vincent, "Measurement of coarse aerosols in workplaces: A review," *Analyst*, vol. 119 , 1994.

[5] B. T. Chen and H. C. Yeh, "An improved virtual impactor: Design and performance," *J. Aerosol Sci.*, vol. 18, pp. 203–214, 1987.

[6] W. D. Griffiths, "The selective separation of aerosol particles of different shape," *J. Aerosol Sci.*, vol. 18, pp. 761–763, 1987.

[7] *Human Respiratory Tract Model for Radiological Protection*, vol. 66, Int. Commission Radiolog. Protection, 1994.

[8] J. Porstendorfer, "Properties and behavior of radon and thoron and their decay aparoducts in the air," *J. Aerosol Sci.*, vol. 25, pp. 219–263, 1994.

[9] G. I. Johansson, K. R. Akselsson, P. Eklund, H. C. Hansson, and G. Johsson, "A new technique for the determination of activity distributions of radon daughters," *J. Aerosol Sci.*, vol. 19, pp. 1027–1029, 1988.

[10] D. Y. H. Pui *et al.*, "Electrical aerosol analyzer: Calibration and performance," in *Aerosol Meas.*, D. A. Lundgren *et al.*, Eds. Gainesville, FL: Univ. Florida Press, 1979, pp. 384–399.

[11] S. W. S. McKeever and M. S. Akselrod, "Radiation dosimetry using pulsed optically stimulated luminescence of Al_2O_3:C," *Radiat. Prot. Dosim.*, vol. 84, pp. 317–320, 1999.

[12] E. Bulur and H. Y. Goksu, "Pulsed optically stimulated luminescence from α-Al_2O_3:C using green light emitting diodes," *Radiat. Meas.*, vol. 27, pp. 479–488, 1997.

[13] V. S. Kortov, I. I. Milman, V. I. Kirpa, and J. Lesz, "Some features of α-Al_2O_3:C dosimetric thermoluminescent crystals," *Radiat. Prot. Dosim.*, vol. 55, pp. 279–283, 1994.

[14] M. Moscovitch, R. A. Tawil, and M. Svinkin, "Light induced fading in α-Al_2O_3:C," *Radiat. Prot. Dosim.*, vol. 47, pp. 251–253, 1993.

[15] M. S. Akselrod, N. A. Larsen, V. Whitley, and S. W. S. McKeever, "Thermal quenching of F-center luminescence in Al_2O_3:C," *J. Appl. Phys.*, vol. 84, pp. 3364–3372, 1998.

[16] E. Bulur, H. Y. Goksu, and W. Wahl, "Infrared stimulated luminescence from α-Al_2O_3:C," *Radiat. Meas.*, vol. 29, pp. 625–638, 1998.

[17] S. W. S. McKeever, M. S. Akselrod, and B. G. Markey, "Pulsed optically stimulated luminescence dosimetry using α-Al_2O_3:C," *Radiat. Prot Dosim.*, vol. 65, pp. 267–272, 1996.